Proceedings of the Thirty-third (2023) International Ocean and Polar Engineering Conference **www.isope.org**
Ottawa, Canada, June 19-23, 2023

ISBN 978-1-880653-80-7; ISSN 1098-6189

Development of an Improved Numerical Wave Tank for Wave-Current Interaction Simulations Based on OpenFOAM

*Songtao Chen[1], Linna Wu[2], Weiwen Zhao[1], Decheng Wan[1]**

[1] Computational Marine Hydrodynamics Lab (CMHL), School of Naval Architecture, Ocean and Civil Engineering, Shanghai Jiao Tong University, Shanghai, China
[2] Shanghai Institute of Aerospace System Engineering, Shanghai, China
*Corresponding author

ABSTRACT

In this paper, an improved numerical wave tank based on OpenFOAM is developed for simulations of wave-current interaction. The ghost fluid method (GFM) is implemented to handle the interface jump conditions and eliminate the spurious velocities. The sharp interface is obtained by a fully coupled level set and volume of fluid method (CLSVOF). A modified generating-absorbing boundary condition (GABC) is employed to achieve high-efficiency wave simulations in the presence of uniform currents. At the same time, the stabilized SST k-ω turbulence model is adopted to solve the excessive numerical dissipation in long-time wave propagation. The present numerical model is validated by a benchmark experiment, demonstrating its accuracy in predicting wave elevation and velocity profile.

KEY WORDS: wave-current interaction, ghost fluid method (GFM), coupled level set and volume of fluid method (CLSVOF), generating-absorbing boundary condition (GABC), stabilized SST k-ω turbulence model.

INTRODUCTION

With the rapid development of high-performance computers, Computational Fluid Dynamics (CFD) has been extensively used in marine hydrodynamics. Compared with previous methods like potential flow theory, CFD is more suitable for simulating complex two-phase flows, where violent free surface and large-scale flow separation may coexist. In addition, more detailed flow field information can be provided for in-depth analysis of flow mechanisms.

Given these advantages, many researchers have developed their own two-phase CFD solvers to meet the growing demand for high-fidelity simulations. For the study of wave hydrodynamics, Bihs et al. (2016) developed a three-dimensional numerical wave tank REEF3D based on the level set method and the ghost cell immersed boundary method. To gain a better understanding of wave-structure interaction (WSI), Xie et al. (2020) extended their 3D two-phase flow code (Xdolphin3D) to large eddy simulations. The air-water interface is captured by the high resolution VOF scheme CICSAM, and complex geometries are handled by the Cartesian cut-cell method. Zong et al. (2021) combined their CIP-based numerical model with the adaptive mesh framework Afivo to simulate free-surface flow. The CIP method is used for the spatial discretization of the advection term, and the VOF method THINC/SW is employed for interface capturing. Ferro et al. (2022) developed a GFM-based two-phase solver based on the open source CFD platform OpenFOAM. The Ghost Fluid Method (GFM) is used to deal with interface jump conditions, and several algebraic VOF schemes are implemented to capture the interface instead of the original MULES algorithm.

Based on the CFD approach, many scholars have established various numerical models to study wave-current interaction (WSI), which is common in realistic marine environments. For CFD simulations of wave-current interaction, there are two main approaches to generate combined wave-current conditions. In the case of the first category, the target wave is generated by an internal wave-maker using the mass source term method or the impulse source term method, and the prescribed current is usually achieved through the inlet boundary. For example, Zhang et al. (2014, 2015) used an internal mass source wave-maker and the k-ε turbulence model to simulate two-dimensional wave-current interaction. They systematically studied regular and solitary wave-current interactions from the perspective of current velocity and wave period. Similarly, Hsiao et al. (2020) employed an internal mass source wave-maker and a stabilized k-ε turbulence model to study the wave-current interaction with a sinusoidal bottom based on the open source CFD platform OpenFOAM. Windt et al. (2018) used the Code-Saturne CFD solver to simulate wave-current interaction by adding impulse source terms to the momentum equation. For the second category, the current and wave velocities are superimposed and then specified at the inlet boundary. Compared to the first category, this approach is easier to implement and does not require additional changes to the original solver. Chen and Zou (2019) employed the third-party library waves2Foam to investigate the wave interaction with depth-varying currents, focusing on the effect of vertical current shear. Markus et al. (2013a, 2013b) implemented an in-house wave generator in OpenFOAM 2.1 to study the wave-current interaction between non-linear waves and non-uniform currents (depth-varying exponential velocity profiles). On this basis, they further analyzed structural loadings for tidal stream generators under

such realistic offshore conditions.

In the present study, an improved numerical wave tank for wave-current interaction simulations is presented. The primary objectives are to demonstrate the accuracy of the present numerical model and extend its application to more complex two-phase flows in the near future. The remainder of this paper is organized as follows. First, the numerical methods are introduced in detail, including governing equations, interface capturing method, wave-current generation and turbulence model. Then, the numerical setup for the wave-current simulation is presented. After validating the numerical model with the experimental measurements and numerical results by others, the flow field and the effect of turbulence are analyzed in the following section. Finally, the main conclusions are drawn.

NUMERICAL METHODS

For high-fidelity simulations of marine hydrodynamics, we develop an improved numerical wave tank based on the original two-phase VOF solver interFoam in OpenFOAM. An earlier version of this numerical wave tank has been applied to the wave-structure interaction simulation, demonstrating its good performance in three-dimensional practical problems (Chen et al., 2022). On this basis, several new features have recently been added to this improved solver, further extending its applicability to complex two-phase flows.

Governing equations

When the flow is assumed incompressible with constant density in each phase, the governing equations can be written as:

$$\nabla \cdot \mathbf{U} = 0 , \tag{1}$$

$$\frac{\partial \mathbf{U}}{\partial t} + \nabla \cdot (\mathbf{U}\mathbf{U}) = -\beta \nabla p_d + \nabla \cdot (\nu_{eff} \nabla \mathbf{U}) , \tag{2}$$

where $\mathbf{U}$ is the velocity, $\beta = 1/\rho$ is the inverse density of air or water, $p_d = p - \rho \mathbf{g} \cdot \mathbf{x}$ is the dynamic pressure, p is the total pressure, $\mathbf{g}$ is the gravitational acceleration, and $\mathbf{x}$ is the coordinate vector. $\nu_{eff} = \nu + \nu_t$ is the effective kinematic viscosity, where ν and ν_t are the molecular and eddy viscosities, respectively. Given that the large-scale characteristics in marine hydrodynamics, the surface tension term is neglected in Eq. (2). At the same time, because of the large density ratio between air and water, the pressure jump condition across the interface, i.e., the first term on the RHS of Eq. (2), is handled with the ghost fluid method (GFM). A detailed description of the GFM in the OpenFOAM framework can be found in references (Vukčević et al., 2017; Chen et al., 2022).

Interface capturing method

To obtain a sharp interface, a fully coupled level set and volume of fluid (CLSVOF) method is used instead of the previous algebraic volume of fluid (VOF) method. The transport equations for the volume fraction α and the level set function ϕ are as follows:

$$\frac{\partial \alpha}{\partial t} + \nabla \cdot (\alpha \mathbf{U}) = 0 , \tag{3}$$

$$\frac{\partial \phi}{\partial t} + \nabla \cdot (\phi \mathbf{U}) = 0 \cdot \tag{4}$$

For robustness and boundedness, Eq. (3) is still solved by the MULES (multidimensional universal limiter with explicit solution) algorithm in OpenFOAM. However, in the present method, the high-order volume fraction flux is given using the geometric reconstruction concept of the piecewise-linear interface calculation (PLIC) instead of the conventional TVD schemes. In the interface reconstruction step, the normal vector of the cutting plane in each cell can be accurately calculated by the level set function field. For detailed information about this method, refer to the references (Dianat et al., 2017; Chen et al., 2023).

Wave-current generation

In our previous study, the generating-absorbing boundary condition (GABC) method (Wellens and Borsboom, 2020; Borsboom and Jacobsen, 2021) was modified within the GFM framework, and satisfactory results were obtained in terms of wave generation and absorption. The GABC method is based on the classical Sommerfeld radiation condition and can finally be written in the form of the dynamic pressure boundary condition:

$$\left(1 + \frac{c(z)}{\Delta}\left(\frac{1}{a_p}\right)_b\right)\left(p_d\right)_b = \frac{c(z)}{\Delta}\left(\frac{1}{a_p}\right)_b \left(p_d\right)_C + \frac{c(z)}{\beta_w}\frac{\left(\mathbf{H}(\mathbf{U}_N)\right)_b}{\left(a_p\right)_b} - S^G , \tag{5}$$

where $c(z) = \sqrt{gh}a(z)$, h is the water depth, and $a(z)$ is a depth-varying function instead of a constant value a. Δ is the distance between the boundary face center and the adjacent owner cell center, $()_b$ denotes the variables on the boundary face, $()_C$ denotes the variables of the owner cell of the boundary face, and a_p is the diagonal coefficient of the semi-discretized form of Eq. (2). $\mathbf{H}(\mathbf{u}_N) = -\sum_f a_N \mathbf{u}_N + \mathbf{b}$ consists of the source term $\mathbf{b}$ arising from the discretization of Eq. (2) and the contribution $-\sum_f a_N \mathbf{u}_N$ from all neighbor cells, a_N is the off-diagonal coefficient of the semi-discretized form of Eq. (2), $\mathbf{u}_N$ is the velocity of the neighbor cell, β_w is the inverse water density, and S_G is the source term for wave generation.

In this study, the presence of uniform current is further considered in the GFM method (Chang, 2021), enabling the simulation of combined wave-current conditions. When the uniform current is introduced, Eq. (5) then becomes:

$$\left(1 + \frac{c(z)}{\Delta}\left(\frac{1}{a_p}\right)_b\right)\left(p_d\right)_b = \frac{c(z)}{\Delta}\left(\frac{1}{a_p}\right)_b \left(p_d\right)_C + \frac{c(z)}{\beta_w}\frac{\left(\mathbf{H}(\mathbf{U}_N)\right)_b}{\left(a_p\right)_b} - \frac{c(z)}{\beta_w}\mathbf{u}_{\mathbf{current}} \cdot \mathbf{n}_{\mathbf{b}} - S^G , \tag{6}$$

where $\mathbf{u}_{\mathbf{current}}$ is the uniform velocity vector, and $\mathbf{n}_{\mathbf{b}}$ is the unit normal vector of the boundary face.

Turbulence model

In the present study, a stabilized k-ω SST model (Larsen and Fuhrman, 2018; Devolder et al., 2017) is employed to overcome excessive numerical dissipation in wave propagation problems. Compared to the original k-ω SST model (Menter et al., 2003), this stabilized variant solves the overestimated eddy viscosity near the interface. The transport equations for the turbulence kinetic energy k and the turbulence specific dissipation ω are as follows:

$$\frac{\partial \rho k}{\partial t}+\nabla\cdot\left(\rho\mathbf{U}k\right)=\nabla\cdot\left[\left(\mu+\sigma_k\mu_t\right)\nabla k\right]+P_k-\rho\beta^*k\omega-\frac{\nu_t}{\sigma_t}\nabla\rho\cdot\mathbf{g}\quad, \tag{7}$$

$$\frac{\partial \rho \omega}{\partial t}+\nabla\cdot\left(\rho\mathbf{U}\omega\right)=\nabla\cdot\left[\left(\mu+\sigma_\omega\mu_t\right)\nabla\omega\right]+\rho P_\omega-\rho\beta\omega^2 +2\left(1-F_1\right)\frac{\sigma_{\omega 2}}{\omega}\nabla k\cdot\nabla\omega\quad, \tag{8}$$

where $\widetilde{P_k}$ is the production term for k, σ_t is the coefficient of the buoyancy production term, P_ω is the production term for ω, F_1 is the blending function, and σ_k, σ_ω, β^*, $\sigma_{\omega 2}$ are all constants. The eddy viscosity is defined as:

$$\nu_t=\frac{a_1 k}{\max\left(a_1\omega, F_2\sqrt{p_0}, a_1\lambda_2\frac{\beta}{\beta^*\alpha}\frac{p_0}{p_\Omega}\omega\right)}, \tag{9}$$

where F_2 is another blending function, p_0 is the square of the mean strain rate tensor, and p_Ω is the square of the mean rotation rate tensor.

NUMERICAL SETUP

The focus of the present study is to validate the improved numerical wave tank by comparing it with the laboratory experiments of Umeyama (2011). The experiments were performed in a wave channel with main dimensions of 25.0 m × 0.7 m × 1.0 m (length × width × depth). At the ends of the channel, a piston-type wave maker and a wave absorber were placed for wave generation and absorption, respectively. In addition, a pipe under the tank was employed to recirculate the water, generating the target uniform currents. More details about the experimental facilities can be found in the reference (Umeyama, 2011).

Computational domain and mesh

To save computational cost, a two-dimensional computational domain of $0 < x < 13$ m and -0.3 m $< z < 0.3$ m is adopted in our simulation, as shown in Fig. 1. The still water is located at $z = 0$, and the water depth h is set to 0.3 m, the same as in the experiments. The top of the computational domain, the atmosphere boundary, is 0.3 m above the still water.

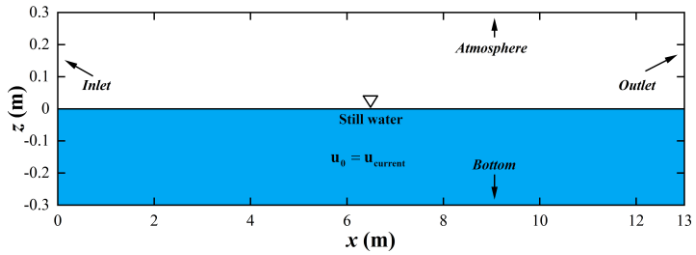

Fig. 1. Computational domain.

Fig. 2 shows the computational mesh. In the horizontal direction, the mesh has a uniform length $\lambda/\Delta x \approx 130$, with approximately 130 cells per wavelength λ. In the vertical direction, the mesh is refined near the interface and bottom boundary, as shown in the enlargements of Fig. 2. To ensure the accuracy in long-time wave propagation, the number of cells per wave height is set to $H/\Delta z \approx 30$. Besides, considering the intermediate depth condition, the height of the first layer at the bottom boundary is set to $\Delta z \approx 1/240\ h$, and the expansion ratio is set to 1.05. After that, the mesh finally consists of 2.028×10^5 cells.

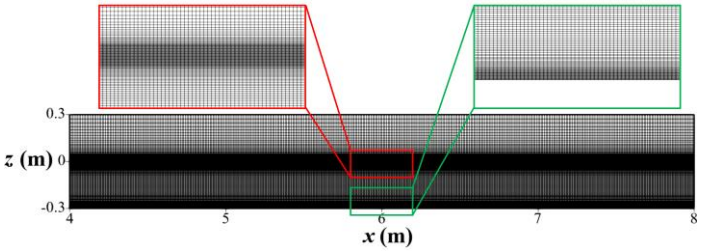

Fig. 2. Computational mesh.

Boundary and initial conditions

As for the boundary conditions, the GABC is applied to the inlet and outlet for wave generation and absorption, respectively. The no-slip boundary condition is imposed on the bottom, the Neumann boundary condition $\partial\varphi/\partial n = 0$ is used for the atmosphere, and the empty boundary condition is adopted for the lateral sides (not shown in Fig. 1).

According to the experiments, the input wave height H is 0.0361 m and the wave period T is 1 s. The uniform current $\mathbf{u}_{current}$ is set to (0.08, 0, 0) m/s, in the same direction as the wave propagation. At the beginning of the simulation, the still water is initialized with $\mathbf{u}_{current}$ to save time to reach stable state. For the variables of the turbulence model, the eddy viscosity is initially set to $\nu_t/\nu = 1$, following the settings of Larsen and Fuhrman (2018). The turbulence specific dissipation is initially set to $\omega = 2.71\sqrt{p_0}$, where p_0 is calculated as 0.89 s^{-2}. Correspondingly, the turbulence kinetic energy is initialized with $k = \omega\nu_t$.

The temporal discretization is performed using a blended scheme with a blending factor of 0.95 (Zhuang and Wan, 2021), which is between the first-order Euler scheme and the second-order Crank-Nicolson scheme. For the spatial discretization, the advection term and the diffusion term are discretized using a second-order linearUpwind scheme and a second-order linear scheme, respectively. Among them, the diffusion term of the pressure Poisson equation is specially discretized using a second-order GFM-corrected linear scheme, and the advection term of the level set function transport equation is discretized using a second-order vanLeer TVD scheme. The time step is set to $\Delta t = 1/400\ T$, satisfying that the maximum Courant number is less than 0.5. The total simulation time t is 50 T, which guarantees enough periodic stable results for statistical analysis.

RESULTS AND DISCUSSION

Numerical validation

Fig. 3 shows the comparison of phase-averaged surface elevations in a wave period. The numerical results at $x = 6$ m for the last 20 wave cycles are collected and averaged in our statistical analysis. It can be seen that the present result is in good agreement with the laboratory experiment and the numerical simulation by Zhang et al. (2014). However, a slight discrepancy can be found near the wave crest, where the crest height is over-estimated. It may require further improvements to our numerical model. Fig. 4 further compares the instantaneous horizontal velocity

profiles at different time instants with a time interval of 0.25s. For comparison, only the velocity in the water column ($\phi > 0$) of the last wave cycle is shown. It shows that the present numerical model can accurately predict the horizontal velocity through the whole water column under wave-current interaction. The over-estimated wave crest in Fig. 3 is responsible for the discrepancy in Fig. 4(c), where the numerical prediction is higher than the experimental measurement. On the other hand, our numerical model shows better performance in predicting the velocity near the bottom. Compared with the numerical results of Zhang et al. (2014), the boundary layer on the bottom becomes thicker (velocity gradient becomes gentler) in our simulation, which agrees better with the experiment. This difference can be attributed to two possible aspects: the simulation time and the turbulence model. According to a numerical study of the current-only case by Windt et al. (2018), the boundary layer thickness increases with the simulation time, and a stable velocity profile can only be obtained after 40s. In contrast, the total simulation time of Zhang et al. (2014) is only 25s, where the last 5 wave cycles (5s) are used for the analysis. Besides, Zhang et al. (2014) adopted the k-ε turbulence model, whereas we used a stabilized SST k-ω turbulence model in the present study. The performance of different turbulence models in boundary layer flows may also account for this difference.

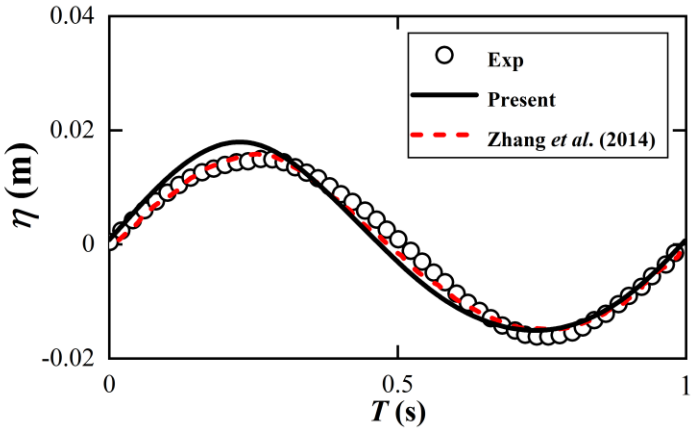

Fig. 3. Comparison of phase-averaged surface elevations in a wave period.

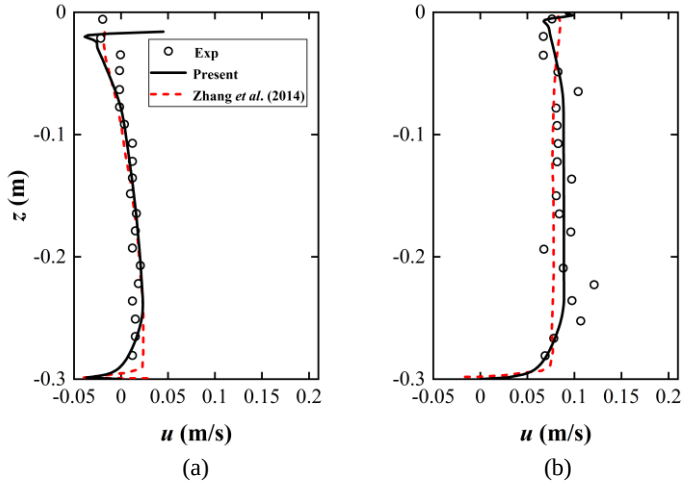

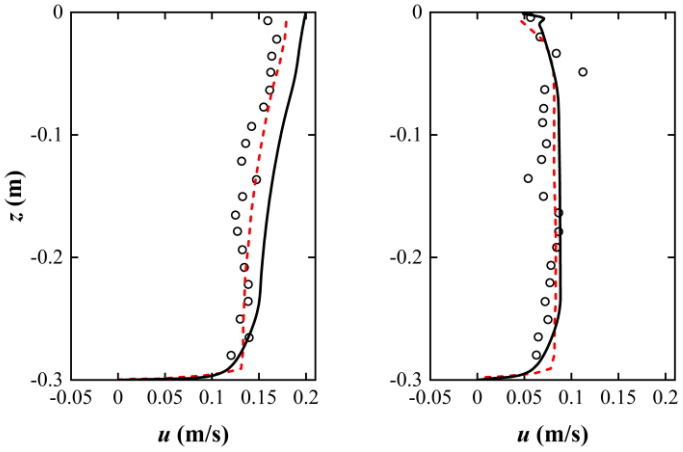

Fig. 4. Comparison of instantaneous horizontal velocity profiles at (a) t = 0, (b) t = 0.25 s, (c) t = 0.5 s, and (d) t = 0.75 s.

Flow field analysis

Fig. 5 shows the instantaneous horizontal velocity contours at different time instants. The solid black line is the instantaneous free surface, represented by the contour line of ϕ = 0. Due to the use of the GFM, the reported spurious air velocities (Afshar, 2010) are significantly reduced, leading to a more physical flow field. In addition, a small recirculation zone can be observed on the bottom below the wave trough, which can also be seen in Fig. 4(a). Fig. 6 illustrates the instantaneous level set function contour at t = 0.5 s. It can be clearly observed that the signed distance property of the level set function is well preserved, demonstrating the effectiveness of the present CLSVOF method.

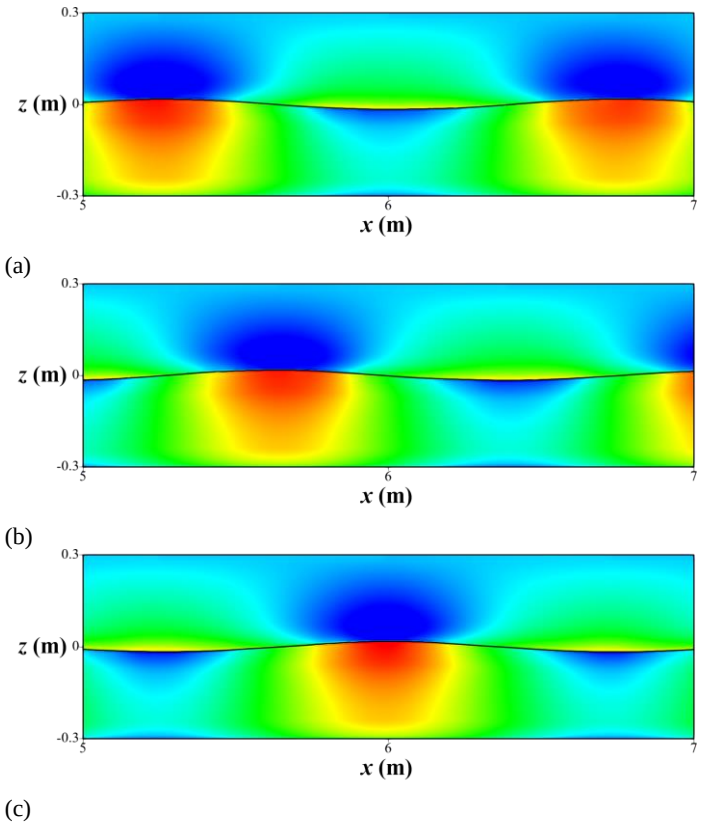

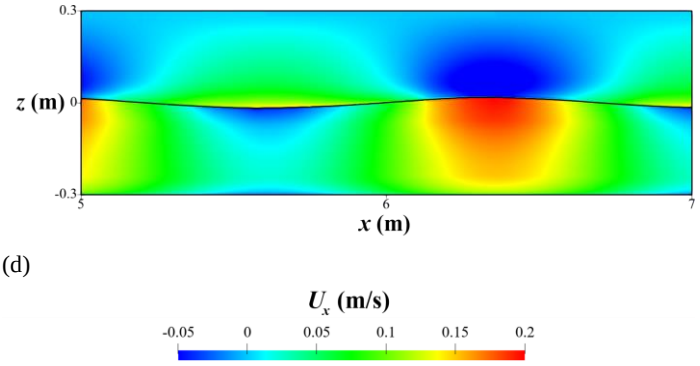

(d)

Fig. 5. Horizontal velocity contours at (a) t = 0, (b) t = 0.25 s, (c) t = 0.5 s, and (d) t = 0.75 s.

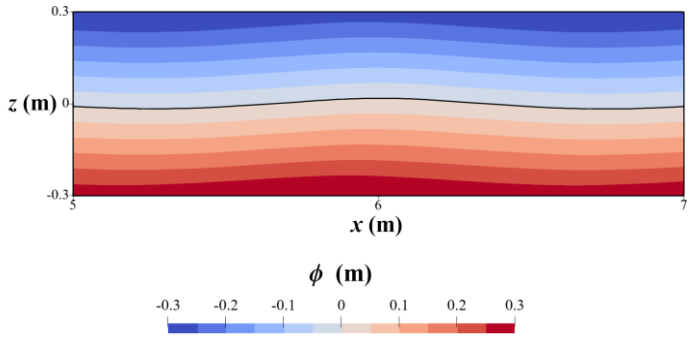

Fig. 6. Level set function contour at t = 0.5 s.

Effect of turbulence

In the above simulation, the stabilized SST k-ω model is adopted to account for the turbulence effect. To better demonstrate its superiority in wave-current interaction, the laminar model and the original SST k-ω model are also used to perform the simulation under the same working condition. Among them, the initial conditions and wall functions of the original SST k-ω model are kept the same as those of the stabilized k-ω model. Fig. 7 shows the comparison of phase-averaged surface elevations in a wave period using different turbulence models. It can be seen that the laminar model shows almost the same result as the stabilized SST k-ω model. However, the original SST k-ω model significantly underestimates the amplitude of the surface elevation, which can be explained by the over-predicted eddy viscosity near the free surface. In addition, the phase of the original SST k-ω model is also slightly different from the previous ones.

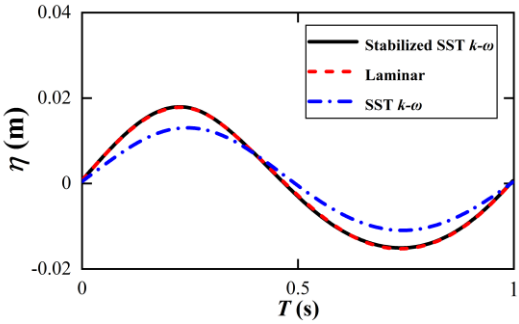

Fig. 7. Comparison of phase-averaged surface elevations in a wave period using different turbulence models.

Fig. 8 compares the instantaneous horizontal velocity profiles of different turbulence models. The comparison shows that the laminar model gives almost the same result as the stabilized SST k-ω model in the mid-depth region but is slightly different near the bottom and the free surface. The laminar model underpredicts the thickness of the boundary layer on the bottom while showing slow recovery near the free surface. This feature suggests that the laminar model may be suitable for deep water conditions, where the bottom effect can be ignored. On the other hand, due to the significant differences in surface elevation, especially at the wave crest and trough (as shown in Fig. 8(a) and (c)), the original SST k-ω model cannot give satisfying results. It further demonstrates that the original SST k-ω model cannot be used for the numerical simulation of wave-current interaction. To further illustrate the reason, Fig. 9 and Fig. 10 present the comparison of turbulence kinetic energy and eddy viscosity, respectively. As shown in Fig. 9, the stabilized SST k-ω model significantly resolves the overproduction of turbulence kinetic energy near the free surface due to the inclusion of the buoyancy production term in Eq. (7). Also, under the combined action of the buoyancy production term and the eddy viscosity limiter, the excessive generation of eddy viscosity near the free surface is significantly improved, as shown in Fig. 10. Moreover, Fig. 10(b) shows that the eddy viscosity is mainly distributed near the bottom and the free surface, which can well explain the difference between the laminar model and the present stabilized model in Fig. 8.

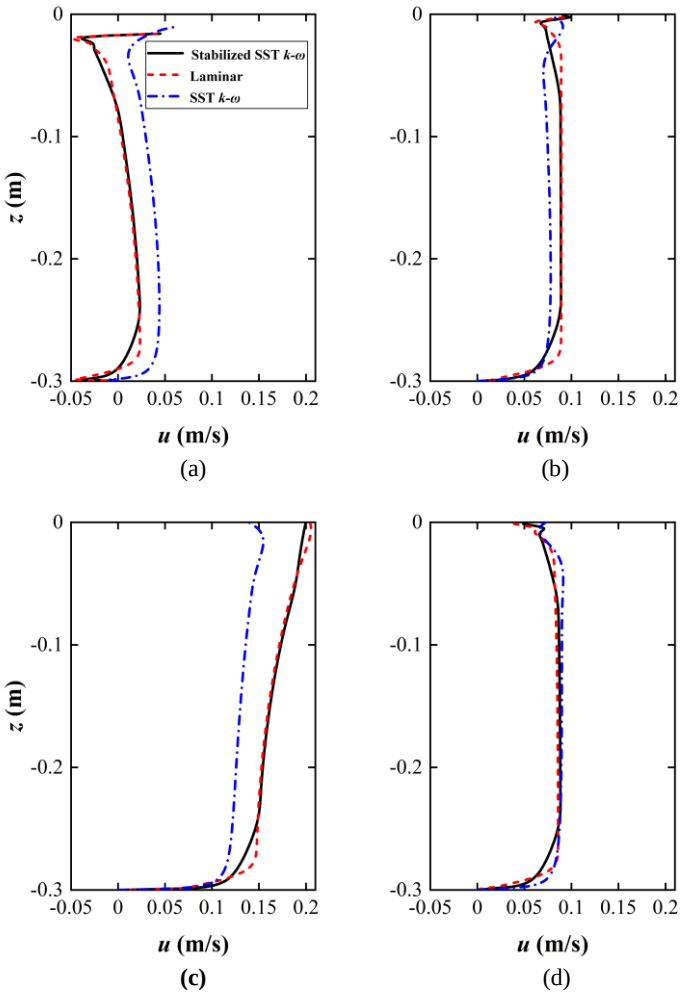

Fig. 8. Comparison of instantaneous horizontal velocity profiles using different turbulence models at (a) t = 0, (b) t = 0.25 s, (c) t = 0.5 s, and (d) t = 0.75 s.

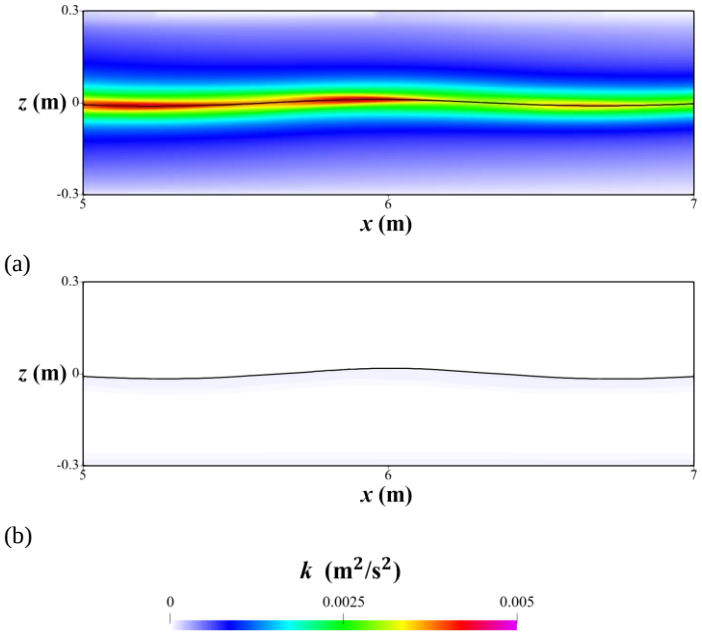

Fig. 9. Comparison of turbulence kinetic energy at t = 0.5 s: (a) SST k-ω and (b) Stabilized SST k-ω.

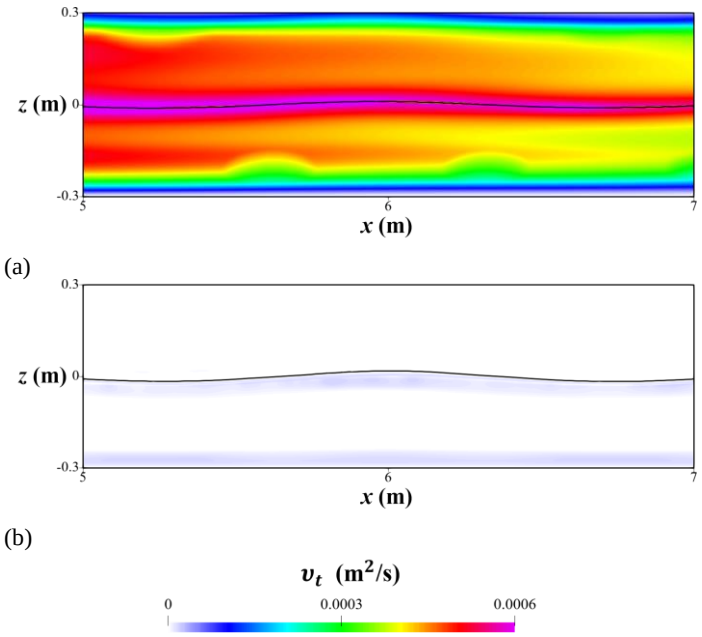

Fig. 10. Comparison of eddy viscosity at t = 0.5 s: (a) SST k-ω and (b) Stabilized SST k-ω.

CONCLUSIONS

In this paper, an improved numerical wave tank based on OpenFOAM is developed and applied to a two-dimensional simulation of wave-current interaction. The GFM is used to eliminate the reported spurious air velocities, and a fully CLSVOF method is implemented to capture the sharp interface. For wave-current generation and absorption, an efficiency method, a modified GABC approach, is employed to achieve wave propagation with uniform current. In addition, a stabilized SST k-ω model is adopted to account for the turbulence effect in wave-current interaction. The present numerical results are first compared with experimental measurements and then analyzed for the flow field. Furthermore, the effect of turbulence is discussed by comparing the results of different models. The main conclusions are as follows.

The numerical results are in good agreement with the experimental data in terms of surface elevation and horizontal velocity profile, which proves the accuracy of the present numerical model. Moreover, our numerical model performs better in predicting the velocity profile near the bottom. For the flow field, the implementation of the GFM eliminates the spurious air velocities, and the current CLSVOF method is effective in capturing the interface. Compared with the stabilized SST k-ω model, the original SST k-ω model under-predicts the surface elevation due to the excessive generation of turbulence kinetic energy and eddy viscosity near the free surface. As a result, the velocity profiles also show a large discrepancy. On the other hand, the laminar model is sufficient to predict the surface elevation in wave-current interaction while showing slight differences in the velocity profiles near the bottom and the free surface. In the future, we will apply this improved numerical wave tank to other complex two-phase flows in marine hydrodynamics and study their flow mechanisms.

ACKNOWLEDGEMENTS

This work was supported by the National Natural Science Foundation of China (52131102), and the National Key Research and Development Program of China (2019YFB1704200), to which the authors are most grateful.

REFERENCES

Afshar, MA (2010). “Numerical wave generation in OpenFOAM®,” Master of Science Thesis, Chalmers University of Technology.

Bihs, H, Kamath, A, Chella, MA, Aggarwal, A, and Arntsen, ØA (2016). “A new level set numerical wave tank with improved density interpolation for complex wave hydrodynamics,” *Computers and Fluids*, 140, 191-208.

Borsboom, M, and Jacobsen, NG (2021). “A generating-absorbing boundary condition for dispersive waves,” *International Journal for Numerical Methods in Fluids*, 93, 2443–2467.

Chang, X (2021). “An absorbing boundary condition for wave-current flow simulations in maritime applications,” PhD Thesis, Delft University of Technology.

Chen, H, and Zou, Q (2019). “Effects of following and opposing vertical current shear on nonlinear wave interactions,” *Applied Ocean Research*, 89, 23-35.

Chen, S, Zhao, W, and Wan, D (2022). “On the scattering of focused wave by a finite surface-piercing circular cylinder: A numerical investigation,” *Physics of Fluids*, 34(3), 035132.

Chen, S, Zhao, W, and Wan, D (2023). “Implementation of the coupled level set and volume of fluid method in OpenFOAM: A comparison with existing VOF techniques,” *In Proceedings of the 11th International Conference on Multiphase Flow*, Kobe, Japan, April 2-7.

Devolder, B, Rauwoens, P, and Troch, P (2017). “Application of a buoyancy-modified k-ω SST turbulence model to simulate wave run-up around a monopile subjected to regular waves using OpenFOAM®,” *Coastal Engineering*, 125, 81-94.

Dianat, M, Skarysz, M, and Garmory, A (2017). “A Coupled Level Set and Volume of Fluid method for automotive exterior water

management applications," *International Journal of Multiphase Flow*, 91, 19-38.

Ferro, P, Landel, P, Pescheux, M, and Guillot, S (2022). "Development of a free surface flow solver using the Ghost Fluid Method on OpenFOAM," *Ocean Engineering*, 253, 111236.

Hsiao, Y, Tsai, CL, Chen, YL, Wu, HL, and Hsiao, SC (2020). "Simulation of wave-current interaction with a sinusoidal bottom using OpenFOAM," *Applied Ocean Research*, 94, 101998.

Larsen, BE, and Fuhrman, DR (2018). "On the over-production of turbulence beneath surface waves in Reynolds-averaged Navier–Stokes models," *Journal of Fluid Mechanics*, 853, 419-460.

Markus, D, Hojjat, M, Wüchner, R, and Bletzinger, KU (2013a). "A CFD approach to modeling wave-current interaction," *International journal of offshore and polar engineering*, 23(01), 29–32.

Markus, D, Wüchner, R, and Bletzinger, KU (2013b). "A numerical investigation of combined wave–current loads on tidal stream generators," *Ocean engineering*, 72, 416-428.

Menter, FR, Kuntz, M, and Langtry, R (2003). "Ten years of industrial experience with the SST turbulence model," *Turbulence, heat and mass transfer*, 4(1), 625-632.

Umeyama, M (2011). "Coupled PIV and PTV measurements of particle velocities and trajectories for surface waves following a steady current," *Journal of waterway, port, coastal, and ocean engineering*, 137(2), 85-94.

Vukčević, V, Jasak, H, and Gatin, I (2017). "Implementation of the Ghost Fluid Method for free surface flows in polyhedral Finite Volume framework," *Computers & fluids*, 153, 1-19.

Wellens, P, and Borsboom, M (2020). "A generating and absorbing boundary condition for dispersive waves in detailed simulations of free-surface flow interaction with marine structures," *Computers and Fluids*, 200, 104387.

Windt, C, Davidson, J, Schmitt, P, and Ringwood, JV (2018). "Development of an impulse–source–based wave-current interaction model," *In 6th ECCOMAS European Conference on Computational Mechanics: Solids, Structures and Coupled Problems, ECCM 2018 and 7th ECCOMAS European Conference on Computational Fluid Dynamics, ECFD 2018*, Glasgow, UK, June 11-15, pp. 3202-3212.

Xie, Z, Stoesser, T, Yan, S, Ma, Q, and Lin, P (2020). "A Cartesian cut-cell based multiphase flow model for large-eddy simulation of three-dimensional wave-structure interaction," *Computers and Fluids*, 213, 104747.

Zhang, JS, Zhang, Y, Jeng, DS, Liu, PF, and Zhang, C (2014). "Numerical simulation of wave–current interaction using a RANS solver," *Ocean Engineering*, 75, 157-164.

Zhang, J, Zheng, J, Jeng, DS, and Guo, Y (2015). "Numerical Simulation of Solitary-Wave Propagation over a Steady Current," *Journal of Waterway, Port, Coastal, and Ocean Engineering*, 141(3), 04014041.

Zhuang, Y, and Wan, D (2021). "Parametric study of a new HOS-CFD coupling method," *Journal of Hydrodynamics*, 33(1), 43-54.

Zong, Y, Zhao, X, Sun, H, and Zhu, R (2021). "An improved CIP-based numerical model for simulating free-surface flow with adaptive mesh," *Ocean Engineering*, 239, 109840.